SAND2014-15688C

Mapping of Radiation-Induced Resistance Changes and Multiple Conduction Channels in TaO_x Memristors

David R. Hughart, *Member, IEEE*, Jose L. Pacheco, Andrew J. Lohn, Patrick R. Mickel, Edward Bielejec, Gyorgy Vizkelethy, Barney L. Doyle, Steven L. Wolfley, Paul E. Dodd, *Fellow, IEEE*, Marty R. Shaneyfelt, *Fellow, IEEE*, Michael L. McLain, *Member, IEEE*, and Matthew J. Marinella, *Member, IEEE*

***Abstract*—The locations of conductive regions in TaO_x memristors are spatially mapped using a microbeam and Nanoimplanter by rastering an ion beam across the device while monitoring the resistance of the device. Microbeam irradiation with 800 keV Si ions revealed multiple sensitive regions around the perimeter of the devices. The rest of the active device area was found to be insensitive to the ion beam. Nanoimplanter irradiation with 200 keV Si ions demonstrated the ability to more accurately map the size of a sensitive area with a beam spot size of 40 nm by 40 nm. Isolated single spot sensitive regions were observed to evolve into larger sensitive region that extends approximately 240 nm.**

***Index Terms*—Memristor, resistive memory, RRAM, radiation effects, displacement damage, microbeam, nanoimplanter, tantalum**

I. Introduction

Resistive RAM (ReRAM) is one of the leading candidates to replace current memory technologies as they become increasingly limited by scaling. Many companies are actively researching ReRAM production and Panasonic has already released a commercially available embedded 8-bit MCU. ReRAM is composed of memristors, devices that can change resistance based on applied current and voltage, resulting in a hysteresis loop like the example plotted in Fig. 1(a) along with a cross section of a typical device in Fig. 1(b). A memristor structure usually consists of two metal terminals with an insulator between them. Tantalum and hafnium oxide are leading candidates for the insulator material.

Initial radiation studies have been promising for tantalum [1, 2], titanium [3, 4], and hafnium [5-7] devices. Previous work on similar TaO_x memristors showed gradual resistance degradation with increasing fluence of 800 keV Si and Ta ions [1, 2]. The resistance likely degrades when oxygen vacancies are introduced because the resistance of the device is determined by the radius and concentration of oxygen vacancies in a localized channel region [8-10].

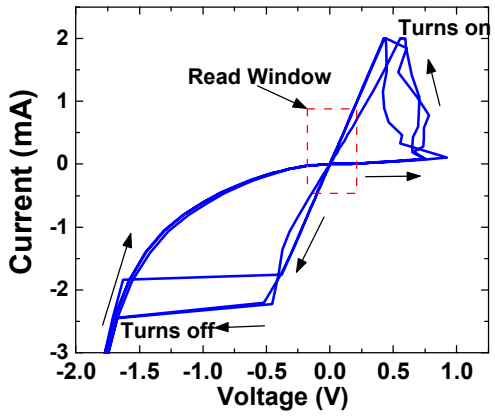

(a)

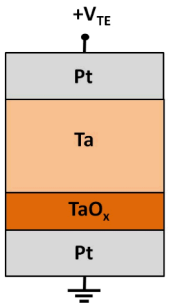

(b)

Fig. 1. (a) Typical I-V curve for a TaO_x memristor with an example "read window" drawn. Multiple loops are plotted [1]. (b) A cross section of a typical memristor used for microbeam irradiations. For the Nanoimplanter irradiation, the stack was inverted so that the Ta layer is below the oxide.

Manuscript received July 12, 2014. This work was supported in part by Sandia National Laboratory's Laboratory Directed Research and Development (LDRD) Program and the Defense Threat Reduction Agency. Sandia National Laboratories is a multi-program laboratory managed and operated by Sandia Corporation, a wholly owned subsidiary of Lockheed Martin Corporation, for the U.S. Department of Energy's National Nuclear Security Administration under contract DE-AC04-94AL85000.

D. R. Hughart, J. L. Pacheco, A. J. Lohn, P. R. Mickel, P. E. Dodd, M. R. Shaneyfelt, E. Bielejec, G. Vizkelethy, B. L. Doyle, S. L. Wolfley, M. L. McLain, and M. J. Marinella are with Sandia National Laboratories, Albuquerque, NM 87185 USA (phone: 505-844-3153; e-mail: dhughar@sandia.gov).

In this work we use a nuclear microbeam to target individual areas of TaO_x memristors using 800 keV Si ions. We find that there are multiple sensitive areas, but that most significant resistance changes occur in a limited number of areas, all of which are located on the perimeter of the device area. This demonstrates that only certain areas of the device may be vulnerable to radiation-induced resistance changes due to displacement damage. This may explain why the decreases in resistance in previous works were gradual and inconsistent [1, 2], since an ion must strike a critical region.

We also use Sandia's Nanoimplanter to target individual areas of a TaO_x memristor with even greater precision using 200 keV Si ions. We find a sensitive region on the edge of the device and are able to measure the size of the sensitive area, which grows from two isolated spots of at most 40 nm × 40 nm (the resolution of our measurement) to a spot that extends approximately 240 nm in a single direction.

II. Experimental Details

TaO_x memristors used in this study were defined by "dogbone" electrodes where a bit stack is deposited between top and bottom electrodes aligned in perpendicular directions. The active device area is located where the electrodes cross. The memristors irradiated in the microbeam had a 30 nm Pt bottom electrode, a TaO_x insulating layer thickness of approximately 10 nm, and a top electrode composed of 50 nm Ta and then 10 nm Pt. The memristors irradiated with the Nanoimplanter had a 50 nm Pt and 50 nm Ta bottom electrode, a TaO_x insulating layer thickness of approximately 10 nm, and a 50 nm Pt top electrode. This stack will be referred to as an inverted stack since the Ta/Pt electrode is on the bottom. These parts were characterized with the opposite polarity voltage/current because of the reversed electrode structure.

For the microbeam tests, memristor die were packaged in standard 28 pin DIPs; a typical sample had six devices bonded. Prior to irradiation, individual devices were repeatedly set and reset to test for instability, where off-state resistance changes over time until it is similar to the on-state resistance [11]. Devices that showed degradation in off-state resistance pre-irradiation were discarded in order to ensure that changes in device characteristics were due to irradiation.

Electrical measurements were made using an Agilent 4156C Semiconductor Parameter Analyzer. During the irradiation a constant bias of 50 mV was applied across the device. This bias is low enough that it causes no changes to the resistance state of the devices. A Keithley 428 Programmable Current Amplifier with a gain of 105 V/A was used to convert the current through the device to voltage. The devices were irradiated using the nuclear microbeam on Sandia National Laboratories' Tandem accelerator. An 800 keV Si ion beam was rastered across the device with the resistance being recorded every time the beam moved to the next spot. All measurements were made in vacuum.

For the Nanoimplanter test, an unpackaged memristor die was mounted in the vacuum chamber and electrical connections were established using probes. Electrical measurements were made using an Agilent B1500. During irradiation a constant -50 mV was applied across the device. A Keithley 428 Programmable Current Amplifier with a gain of 105 V/A was used to convert the current through the device to voltage, which was recorded by a Raith ADC. The resistance of the device was measured each time the beam moved to a new spot.

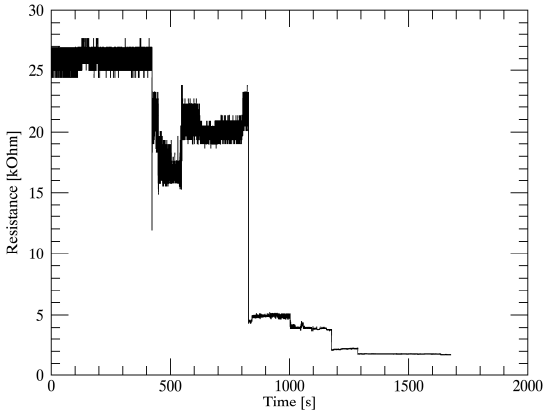

Fig. 2. Resistance vs. time for a 10 μm × 10 μm device over the course of eighty one scans with the microbeam. Dwell time is 200 μs and resistance is measured every time the beam moves.

III. Results

A. Microbeam

The first device (with dimensions 10 μm × 10 μm) was irradiated seven times with the beam repeatedly scanned over the device, and twice with the beam in a stationary position. The spot size was 0.9 μm in the x-direction and 2 μm in the y-direction. The dwell time (the amount of time the beam is targeted at a given spot) was 200 μs. The beam current was approximately 5000 ions per second, resulting in one ion hitting each spot on average. Fig. 2 plots the resistance of the device versus time. Data is noisier at higher resistances because the current through the device is much lower. There are multiple significant decreases in resistance and two significant increases in resistance. A conducting channel in a memristor has a higher oxygen vacancy concentration than the rest of the surrounding oxide [8] and the decreases in resistance are likely due to the creation of oxygen vacancies in a channel region. The increases in resistance may be caused by an ion disrupting the conducting path formed by oxygen vacancies. The device was reset after the first run and this procedure was repeated six more times. Note that between runs two and three, two irradiations were performed with the beam in a stationary location. These irradiations will be discussed after the results for the remaining six scan irradiations are presented. The beam settings for the final six scan runs used a dwell time of 500 μs and the beam current was approximately 9300 ions per second, resulting in four to five ions hitting each spot on average. Fig. 3(a) plots the

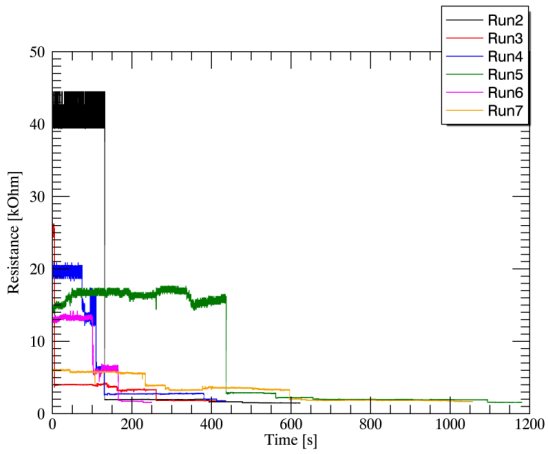

(a)

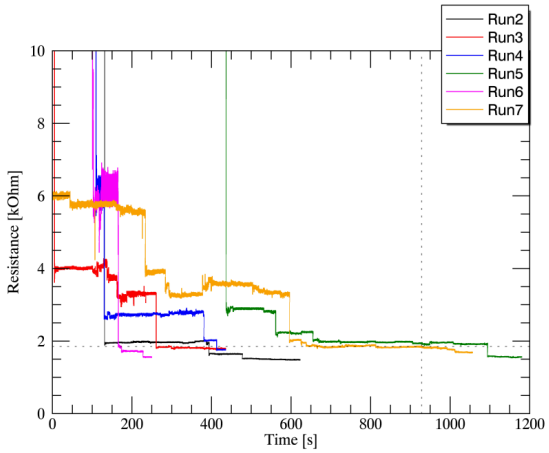

(b)

Fig. 3. (a) Resistance vs. time for the 10 µm × 10 µm device for six different irradiations. The number of scans ranged from ten to forty for various runs. The device was reset between each run. Dwell time is 500 µs and resistance is measured every time the beam moves. (b) Magnification of the data at lower resistances.

remaining six runs on the device and Fig. 3(b) shows a magnification of the lower area of the graph. Each run shows multiple discrete drops in resistance and a gradual reduction in starting off-state resistance. The large decrease in off-state resistance between runs two and three may be related to the two stationary runs performed between them. The size of a conducting channel is likely smaller than the beam spot size, with a diameter that may be on the order of 100 nm [9, 12]. Given that there were generally ten to forty scans of the device per run and five or less significant changes in resistance during the runs, it is likely that even when a critical region was targeted within the spot, ions would not necessarily strike it since the actual charge track of the ion is smaller than the spot size. Thus, the resistance changes seen in Fig. 3 may be due to the effects of single ions even though four to five ions are striking each spot on average.

Fig. 4 plots the location of the beam when each major change in resistance occurred. The rectangle drawn around

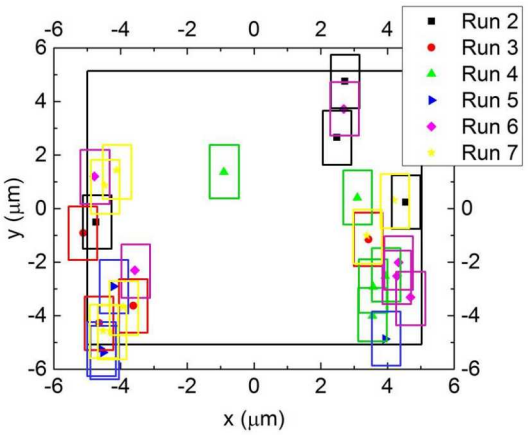

Fig. 4. Location of the beam when resistance changes occurred during runs two through seven of the scan irradiations for the 10 µm × 10 µm device. The rectangles indicate the beam spot size. Black lines mark the edges of the device.

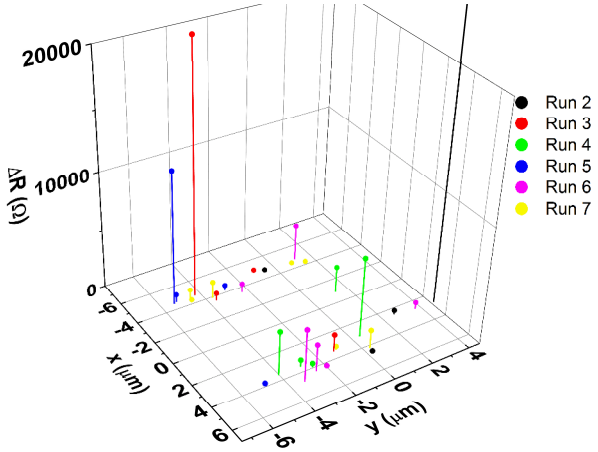

Fig. 5. Location of the beam when resistance changes occurred during runs two through seven of the scan irradiations for the 10 µm × 10 µm device. The z-axis plots the magnitude of the resistance change at that location. The data point from run two that is larger than the scale shown on the graph is a resistance change of 40 kΩ. The scale was cut off at 20 kΩ to preserve the readability of the other data. Spatial coordinates are identical to Fig. 4.

each point represents the size of the beam spot. Most of the resistance changes are clustered around four areas. This indicates that there are multiple areas that may affect the resistance of the device. Fig. 5 plots the locations with the magnitude of the resistance change shown on the z-axis. There are three resistance changes greater than 10 kΩ. Two of the changes (from runs three and five) are near each other and likely from the same channel region. However, a significant change also occurs during run two in an entirely different region of the device. Additionally, there are resistance changes in the range of 3-7 kΩ in other regions of the device during subsequent runs. These results show that there are multiple regions that are sensitive to radiation that can cause significant changes in resistance.

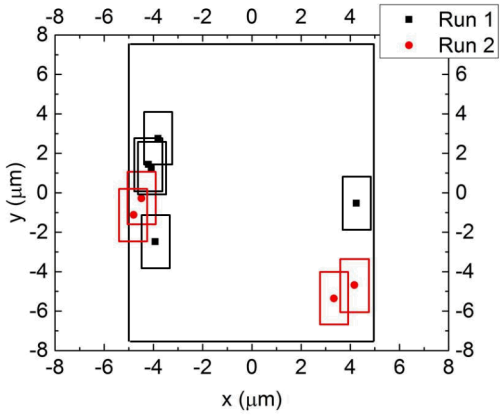

Fig. 6. Location of the beam when resistance changes occurred during two runs of the scan irradiations for the 10 μm × 15 μm device. The rectangles indicate the beam spot size. Black lines mark the edges of the device.

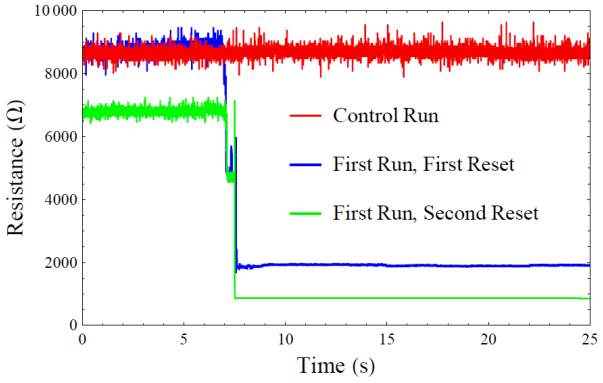

Fig. 7. Resistance vs. time for a 8 μm × 8 μm device over the course of one scan with the Nanoimplanter. The red plot is a control run with the beam blanked. The other two runs show resistance changes at the same time (corresponding to the same location). The device was reset each time after the resistance changed.

Aside from a lone isolated data point, the locations are clustered in areas around the perimeter of the device. To investigate this, the device was irradiated with the beam position held stationary. First, the beam was aimed at the center of the device and allowed to run for 2750 seconds. During this time, the resistance did not change. Next, the beam was positioned in a corner of the device. After 2100 seconds, the resistance decreased from 36 kΩ to 8 kΩ. This result and the location maps in Figs. 4 and 5 suggest that the perimeter is the most sensitive area for the device. Additionally, we irradiated a second memristor (10 μm × 15 μm), performing two runs on the device. Fig. 6 plots the location of the beam when major resistance changes occurred. Once again, the changes occur when the beam is targeting the perimeter of the device.

B. Nanoimplanter

The Nanoimplanter has a smaller target spot size, allowing more precise localization of sensitive areas of the memristors. One 8 μm × 8 μm device with the inverted stack process was irradiated using the Nanoimplanter with a spot size of 40 nm × 40 nm with a step size of 30 nm. Prior to testing, the resistance was monitored with no beam on target to collect control data. Fig. 7 plots the resistance recorded from the control data and the two subsequent runs versus time. Note that there is some noise present in the measurement and that when the part has a high resistance value (as it does in the control data) the current is very low, making the noise a larger percentage of the signal. The changes in resistance that occur during irradiation are significantly larger than the noise present in the control measurement. They also occur at roughly the same time in each run, indicating that the beam is in the same location when the change happens each time. A dwell time of 100 μs was used for the first three runs. The beam current was 0.25 pA, resulting in roughly five ions every six seconds. The part was reset after run two and run three (the device is reset often to maintain a high resistance so that changes due to irradiation are obvious). The dwell time was changed to 50 μs for another set of runs and reset again. During the final set of runs the first two had a dwell time of 50 μs, which was changed to 100 μs for the last run. Fig. 8(a) plots the location of the beam when resistance changes larger than 1.5 kΩ occurred. Note that an exception is made for the third run where multiple smaller changes occur rapidly, effectively making up a larger resistance change, and those smaller individual changes are plotted as well. Fig. 8(b) shows a zoomed view of the most sensitive region. For this device there is a 1 um variation possible in the position and this uncertainty is shown as a lighter shaded area in Fig. 8(a). Most changes occur near the edge, similar to the results seen using the microbeam.

The resistance changes do not occur instantaneously on the previous graphs, instead they stretch out across several measurement points. This is likely a response based on the evolution of the strike that started the change in resistance and not indicative of an extended sensitive area in the X direction (the direction along which the scan progresses). Regardless of the dwell time (how quickly the beam was rastering across the oxide) the approximate duration of the resistance change remained constant at around 6 ms. For consistency, the locations marked in Fig. 8(a) and (b) are those that correspond to the beginning of resistance changes. This may also explain why the X coordinates differ from run to run. If an ion causes a change by striking a critical region, a further strike to that region may be masked by the continued change in resistance from the previous strike.

IV. Discussion

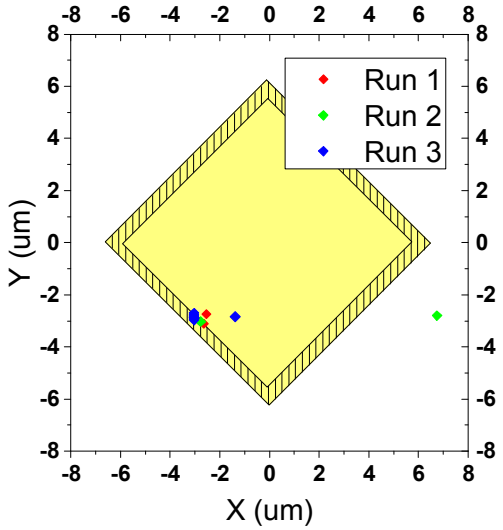

(a)

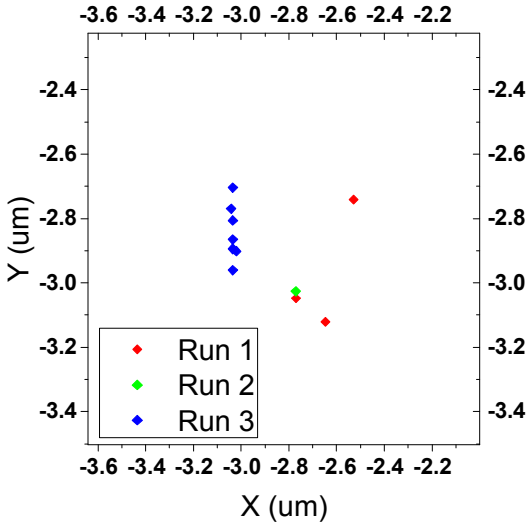

(b)

Fig. 8. (a) Location of the beam when resistance changes occurred during four runs of the scan irradiations using the Nanoimplanter for the 8 µm × 8 µm device. The yellow region indicates the active region. The striped region indicates the 1 um of uncertainly regarding the position of the device. (b) Magnified view of the upper left area of the device.

The size of the sensitive area can be estimated more precisely using the Nanoimplanter. Due to the issue of the extended resistance change in the X direction, the most accurate procedure to estimate the sensitive area size from this data set is to examine where the resistance changes occur in the Y direction and assume that that range is indicative of the diameter of the sensitive area. The size of this region appeared to change after the first two runs. The runs plotted in Fig. 7 show abrupt changes in resistance, but during the third run the device had a rapid succession of smaller changes in resistance that looks like one large change when zoomed out that occur near the same location as the changes during the previous two

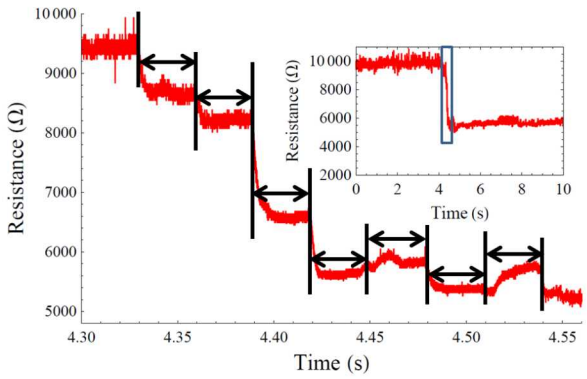

Fig. 9. Magnification of the resistance vs. time plot shown in the inset for a 8 µm × 8 µm device over the course of one scan with the Nanoimplanter. Each change in resistance occurs at roughly equal intervals that correspond to the time it takes to scan one row in the X direction, indicating that each change occurs when the beam is adjacent to the previous spot. All the changes are likely part of one larger sensitive area.

runs. When examining the switching event on a shorter time scale it can be seen that the large change in resistance is actually composed of multiple smaller changes. Fig. 9 plots a large resistance change from the third run in a smaller time window in order to clearly see the multiple changes, which occur every 30 ms. 30 ms is the time it takes to complete one scan and return to the same X value in the next scan, so each change is occurring 30 nm (one step) away in the Y direction from the previous change. This behavior appears to continue for 240 ms (eight iterations) indicating that the sensitive area extends for 240 nm in the Y direction. The fifth and seventh changes actually show increases in resistance (while the rest show decreases), but it is possible that the ion strikes can also disrupt the channel, particularly after a large number of oxygen vacancies have been introduced by the previous strikes. Additionally, the amount of resistance change drops off after the fourth hit, so there may be different degrees of sensitivity and the most critical region may be smaller, extending only roughly 120 nm (the distance between the first four larger changes). The increase in sensitive area from two isolated regions of 40 nm × 40 nm in the first two runs to one much larger region potentially extending 240 nm in a single direction is likely due to the addition of oxygen vacancies during the first two irradiations. However, the size of the filament (and likely the size of the sensitive region) can be changed depending on the applied currents and voltages [13], so operating conditions may affect sensitive area.

In previous papers, irradiation with heavy ions has gradually, but inconsistently, reduced the resistance of memristors [1, 2]. This paper has shown evidence for the existence of insensitive regions of the oxide and has also shown by using the Nanoimplanter that reductions in resistance will consistently occur when the beam is precisely targeting a sensitive region. This suggests that the previous gradual and inconsistent decreases in resistance as well as the high fluence required for their observation may be due to the probability of an ion striking a sensitive region versus an

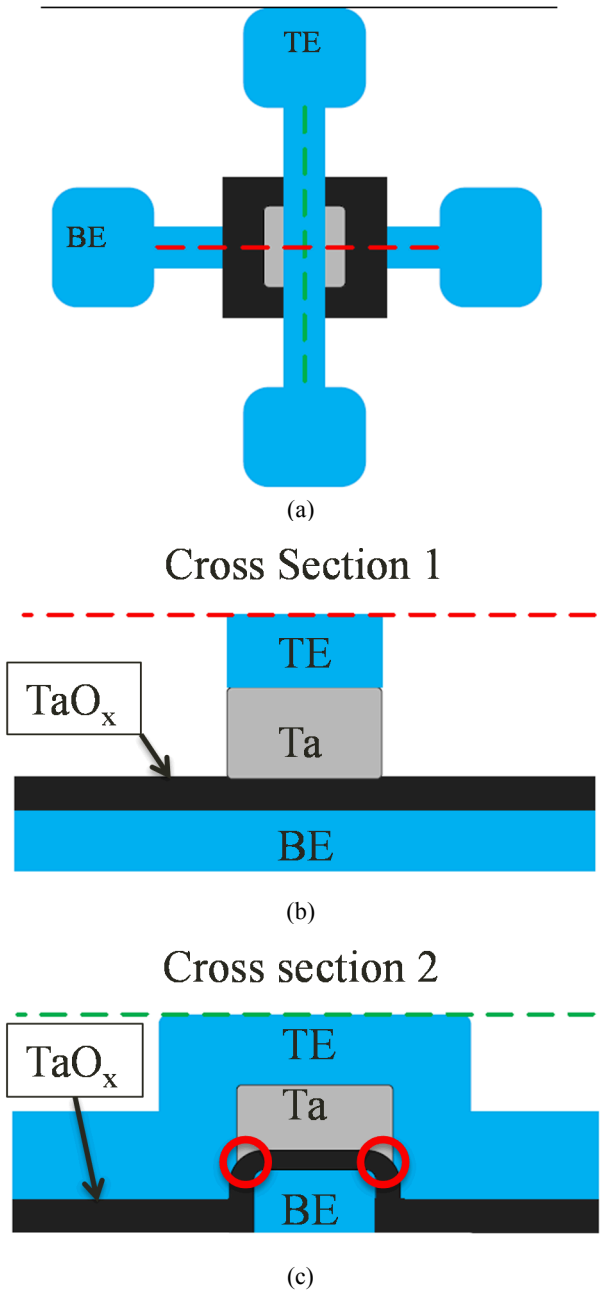

Fig. 10. (a) Overhead schematic of a memristor defined by dogbone electrodes. (b) A cross section along the bottom electrode. (c) A cross section along the top electrode. The edges of the bottom electrode have potential non-conformal areas that are circled in red.

insensitive region. As memristors are scaled down and devices become more densely packed (as they would be in an integrated memory), the fluence required for resistance changes in the same area should decrease significantly.

The memristors tested in this study were most sensitive to ions striking on the perimeter of the active area of the device. This may be due to two factors. First is the convergence of electric field lines near the edge of the device, resulting in a stronger field. Second is that the oxide may be thinner along the edge of the bottom electrode. This is because when the oxide is deposited on the bottom electrode, there may be thickness variations, particularly at the edges where the deposition may not be conformal. This is illustrated in Fig. 10, which shows an overhead view and two cross sections are defined by the black and red cutlines. The edges along the side of the bottom electrode are circled as areas with higher potential for non-uniformity. These factors would likely result in more defects being formed in the perimeter region during forming stress. A recent experiment suggests that multiple channels are initially created during forming [14] and these would then be sensitive during irradiation. It is also possible that only one channel forms, but the perimeter region still has more defects created during forming, making it easier to create a conducting path of defects at the edge. If the formation of the channel can be localized during processing, it may reduce the sensitive area of the device.

V. Conclusion

Radiation sensitive regions in TaO_x memristor oxides have been spatially mapped, demonstrating that there are multiple conduction pathways, or potential conduction pathways, and that a significant portion of the active region is insensitive to radiation. Radiation-sensitive areas tend to preferentially exist around the perimeter of the devices, possibly due to a potentially thinner oxide in that region and the presence of stronger electric fields at the edges during forming that create higher concentrations of defects. The ability to map the location of radiation-sensitive areas down to a resolution of 40 nm × 40 nm nm has been demonstrated. This allowed us to evaluate the size of radiation-sensitive areas of oxide, mapping one sensitive area that may extend up to 240 nm in length. This capability holds much promise to locate and also characterize memristor conduction channels.

Acknowledgement

The authors thank Kathy Myers (Sandia) for packaging and bonding the devices used in this study, Patrick Finnegan (Sandia) for processing memristor wafers, Dan Buller (Sandia) for running the accelerator at Sandia's Ion Beam Laboratory, and Daniel Perry (Sandia) for his assistance in running the Nanoimplanter.

References

[1] M. J. Marinella, S. M. Dalton, P. R. Mickel, P. E. Dodd, M. R. Shaneyfelt, E. Bielejec, G. Vizkelethy, and P. G. Kotula, "Initial assessment of the effects of radiation on the electrical characteristics of TaO_x memristive memories," *IEEE Trans. Nucl. Sci.*, vol. 59, pp. 2987-2994, Dec. 2012.

[2] D. R. Hughart, A. J. Lohn, P. R. Mickel, S. M. Dalton, P. E. Dodd, M. R. Shaneyfelt, A. I. Silva, E. Bielejec, G. Vizkelethy, M. T. Marshall, M. L. McLain, and M. J. Marinella, "A comparison of the radiation response of TaO_x and TiO_2 memristors," *IEEE Trans. Nucl. Sci.*, vol. 60, pp. 4512-4519, Dec. 2013.

[3] W. M. Tong, J. J. Yang, P. J. Kuekes, D. R. Stewart, R. S. Williams, E. DeIonno, E. E. King, S. C. Witczak, M. D. Looper, and J. Osborn, "Radiation hardness of TiO_2 memristive junctions," *IEEE Trans. Nucl. Sci.*, vol. 57, pp. 1640-1643, June 2010.

[4] H. J. Barnaby, S. Malley, M. Land, S. Charnicki, A. Kathuria, B. Wilkens, E. DeIonno, and W. M. Tong, "Impact of alpha particles on the electrical characteristics of TiO_2 memristors," *IEEE Trans. Nucl. Sci.*, vol. 58, pp. 2838-2844, Dec. 2011.

[5] Y. Wang, H. Lv, W. Wang, Q. Liu, S. Long, Q. Wang, Z. Huo, S. Zhang, Y. Li, Q. Zuo, W. Lian, J. Yang, and M. Liu, "Highly stable

radiation-hardened resistive-switching memory," *Elec. Dev. Lett.*, vol. 31, no. 12, pp. 1470-1472, Dec. 2010.

[6] X. He, W. Wang, B. Butcher, S. Tanachutiwat, and R. E. Geer, "Superior TID hardness in TiN/HfO_2/TiN ReRAMs after proton radiation," *IEEE Trans. Nucl. Sci.*, vol. 59, no. 5, pp. 2550-2555, Oct. 2012.

[7] J. S. Bi, Z. S. Han, E. X. Zhang, M. W. McCurdy, R. A. Reed, R. D. Schrimpf, D. M. Fleetwood, M. L. Alles, R. A. Weller, D. Linten, M. Jurczak, and A. Fantini, "The impact of X-ray and proton irradiation on HfO_2/Hf-based bipolar resistive memories," *IEEE Trans. Nucl. Sci.*, vol. 60, no. 6, pp. 4540-4546, Dec. 2013.

[8] P. R. Mickel, A. J. Lohn, B. J. Choi, J. J. Yang, M.-N. Zhang, M. J. Marinella, C. D. James, and R. S. Williams, "A physical model of switching dynamics in tantalum oxide memristive devices," *Appl. Phys. Lett.*, vol. 102, p. 223502, 2013.

[9] F. Miao, J. P. Strachan, J. J. Yang, M.-X. Zhang, I. Goldfarb, A. C. Torrezan, P. Eschbach, R. D. Kelley, G. Medeiros-Ribeiro, and R. S. Williams, "Anatomy of a nanoscale conduction channel reveals the mechanism of a high-performance memristor," *Adv. Mater.* vol. 23, pp. 5633-5640, 2011

[10] J. J. Yang, D. B. Strukov, and D. R. Stewart, "Memristive devices for computing," *Nature Nanotechnology.*, vol. 8, pp. 13-24, 2013.

[11] J. J. Yang, M. X. Zhang, J. P. Strachan, F. Miao, M. D. Pickett, R. D. Kelley, G. Medeiros-Ribeiro, and R.S. Williams, "High switching endurance in TaOx memristive devices," *Appl. Phys. Lett.*, vol. 97, p. 232102, 2010.

[12] J. P. Strachan, G. Medeiros-Ribeiro, J. J. Yang, M.-X. Zhang, F. Miao, I. Goldfarb, M. Holt, V. Rose, and R. S. Williams, "Spectromicroscopy of tantalum oxide memristors," *Appl. Phys. Lett.*, vol. 98, p. 242114, 2011.

[13] P. R. Mickel, A. J. Lohn, C. D. James, and M. J. Marinella, "Isothermal switching and detailed filament evolution in memristive systems," *Adv. Mater.*, vol. 26, pp. 4486-4490, 2014.

[14] G. S. Park, Y. B. Kim, S. Y. Park, X. S. Li, S. Heo, M.-J. Lee, M. Chang, J. H. Kwon, M. Kim, U.-I. Chung, R. Dittmann, R. Waser, and K. Kim, "*In situ* observation of filamentary conducting channels in an asymmetric Ta_2O_{5-x}/TaO_{2-x} bilayer structure," *Nature Communications*, vol. 4, 2013.